Long-Life Pillar[5]quinone Cathode for Aqueous Zinc-Ion Batteries

Serkan Yeşilot, Yasemin Solmaz, Nazmiye Kılıç, Burcu Unal, Ozlem Sel, Rezan Demir-Cakan

LONG-LIFE PILLAR[5]QUINONE CATHODE FOR AQUEOUS ZINC-ION BATTERIES

Serkan Yeşilot[a]*, Yasemin Solmaz[a], Nazmiye Kılıç[a], Burcu Unal[b,c], Ozlem Sel[d,e], Rezan Demir-Cakan[b,c]*

[a] Yasemin Solmaz, Dr. Nazmiye Kılıç, Prof. Serkan Yeşilot
Department of Chemistry
Gebze Technical University
Gebze, Kocaeli, Turkey
E-mail: yesil@gtu.edu.tr

[b] Burcu Unal, Prof. Rezan Demir Cakan
Institute of Nanotechnology
Gebze Technical University
Gebze, Kocaeli, Turkey
E-mail: demir-cakan@gtu.edu.tr

[c] Burcu Unal, Prof. Rezan Demir Cakan
Department of Chemical Engineering
Gebze Technical University
Gebze, Kocaeli, Turkey
E-mail: demir-cakan@gtu.edu.tr

[d] Prof. Ozlem Sel
Chimie du Solide et de l'Energie UMR 8260
Collège de France
75231 Paris Cedex 05, France

[e] Prof. Ozlem Sel
Réseau sur le Stockage Electrochimique de l'Energie (RS2E) CNRS FR 3459,
80039 Amiens Cedex, France

Supporting information for this article is given via a link at the end of the document.

Abstract: Aqueous zinc ion batteries (ZIBs) are currently gaining a significant amount of attention as a low-cost and high safety energy storage option. While mostly inorganic structures are used as cathode materials in aqueous zinc batteries, these materials undergo structural degradation, therefore, alternative organic cathodes are expected to be developed to replace inorganic materials in aqueous zinc ion batteries (AZIBs). In this work, pillar[5]quinone (P5Q) is used as a cathode in AZIBs for the first time. Besides investigating the charge storage mechanism and interfacial property evolution of P5Q by various ex situ analyses, electrochemical quartz crystal microbalance (EQCM) and density functional theory (DFT) demonstrates both Zn^{2+} and H^{+} incorporation. The P5Q exhibits >99% Coulombic efficiency through 10000 cycles at ultra-fast (500 C) current density, yielding a capacity value of approximately 120 mAh g^{-1} at the end of the cycle. When the current density is changed from 500 C to 120 C, an initial discharge capacity of approximately 182 mAh g^{-1} is achieved, demonstrating outstanding performance with over 80% capacity retention for the subsequent 7000 cycles.

Introduction

The energy crisis and energy consumption have become a serious problem today, and current energy systems are based on the use of non-renewable fossil fuels. The detrimental effects of these systems have increased the interest in energy storage systems. [1] Due to their high energy and power density, lithium ion batteries presently dominate the battery industry. While lithium batteries are indispensable for portable devices, interest in alternative battery types is growing as grid applications and large energy storage systems place more emphasis on affordability, reliability and sustainability. [1-2]

In particular zinc rechargeable aqueous batteries (AZIB) are becoming one of the most promising technologies, and are alternatives due to their reliable safety without any risk of flame or explosion, enormous cost competitiveness, environmental friendliness, high theoretical gravimetric and volumetric capacities (820 mAh g^{-1} and 5855 mAh cm^{-3}), low redox potentials (-0.76 V compared to standard hydrogen electrode (SHE)), impressive long-term cycle stability and higher rate capacities. [3] In AZIBs, compounds based on Mn, Co, V and Prussian blue analogues

(PBA) were mostly used as cathodes.[4] These inorganic materials based on transition metals are prohibitively expensive and resources are unevenly distributed geographically, raising concerns about the environment and availability. They also have drawbacks in practical applications, such as their cycle-related instability.[5] Compared to inorganic cathodes, organic cathodes are inexpensive and can be obtained from renewable sources. The designability of organic cathode structures also allows the modification of electrochemical properties such as specific capacity, voltage, electrical conductivity and solubility.[6]

Organic electrode family can be divided into four categories according to their electrochemical properties: organic sulfides, organic radical products, conductive polymers and organic carbonyl compounds. Carbonyl compounds were the first reported among organic electrode materials. [7] Organic carbonyl compound electrodes consist of three different groups. The first of these are structures that have close carbonyls and can form enolate forms through reduction. The second group includes carbonyl structures that are directly bonded to an aromatic structure, and in this group, the distribution of negative charge can be achieved through delocalization. The structures in the third group can create an additional aromatic system through reduction. Quinones, aromatic anhydrides, aromatic imides, and conjugated carboxylates from organic carbonyl compounds are the most commonly used organic electrodes. **[8]** The imine compounds with C=N groups, which are the cathode materials of aqueous ZIBs, also have significant redox activity. During discharge processes, these compounds can be reduced and combine with the cations of the electrolytes, such as Zn^{2+} and H^{+}. Imine compounds often have a long cycle life, a high specific capacity, and fast reaction kinetics. However, their practical applicability is limited since they frequently have a low discharge voltage.[9] Na et al.[10] investigated the effects of Zn^{2+} and H^{+} intercalation/ association with an organic 1,4,5,8-naphthalene diimide (NDI) electrode. They demonstrated that H^{+} intercalation into the NDI electrode is prominent with increasing current rate and favors the dissolution of NDI molecules.[10] π-conjugated aromatic compounds with the imino moiety (=N) are a type of neutral organic base in which (=N) is capable of chelate the proton through a coordination. [11]

Conducting polymers generally display high electronic conductivity due to long p-electron conjugated systems that will contribute to fast redox kinetics. [12] PANI and polypyrrole (PPy) are two types of conducting polymers that have been utilized as aqueous ZIB electrode materials. Zn^{2+} can serve as a cation species in the imine-related redox reaction in Zn/PANI batteries, and counter anions are involved in the interaction between $=NH^{+}$- and -NH- moieties during charging and discharging processes. Conducting polymers often have limited specific capacity (<200 $mAhg^{-1}$) due to low doping levels.[9, 13]

The field of energy storage research has recently been interested in covalent organic frameworks (COF). [14] A new family of porous crystalline polymers called COFs is created by carefully assembling organic building components.[15] For energy storage applications, they offer a complete platform that enables the logical and accurate manipulation of electrochemically active moieties at the molecular level. These characteristics may make COFs attractive electrode materials for ZIBs that can be recharged. Nevertheless, very few academic studies have been conducted to date on the use of COFs as electrode materials for zinc-based batteries.[16]

Among organic cathode materials, quinone compounds, a class of carbonyl compounds, contain two adjacent (or separate) carbonyl groups in a cyclic structure with six unsaturated segments. [4-6] They are low-cost, durable, and high energy density electrode materials due to their high specific capacity, excellent electrochemical reversibility, as well as their molecular diversity and structural adaptability. Their excellent redox activities make them desirable cathode materials for aqueous zinc batteries.[6, 17] Examples of cathode materials in aqueous zinc batteries include tetrachloro-1,4-benzoquinone (p-chloranil), calix[4]quinone (C4Q) and pyrene-4,5,9,10-tetraone (PTO) molecules.[18] Kundu et al.[19] reported a new p-chloranil cathode with crystalline structure for zinc battery, and a capacity of about 200 mAh g^{-1} has been recorded with a flat plateau near 1.1 V of p-chloraniline. Zhao et al. achieved a high specific capacity of 335 mAh g^{-1}, an operating voltage plateau at 1.0 V, and a coulombic efficiency of 93% in aqueous zinc batteries with a cathode of calix[4]quinone (C4Q).[5] The C4Q structure contains eight active carbonyl units, but DFT calculations show that only six carbonyl groups can be actively utilized and this is due to the conical shape of C4Q. In that work, relatively high concentration (3M) zinc salt was used as the electrolyte to reduce solubility. It was also reported that an ion-selective Nafion membrane was used to prevent dissolved discharge products from migrating to the anode side.[5] Guo et al.[20] produced an aqueous zinc battery on the basis of the PTO as the cathode. This PTO cathode was reported to have a capacity of 336 mAh g^{-1} at 0.04 A g^{-1}. Additionally, a cell with a reversible capacity of 145 mAh g^{-1} and a capacity retention rate of 70% after 1000 cycles at a current density of 3 A g^{-1} was demonstrated. Despite this, the PTO is still in its infancy due to its poor electronic conductivity. Although the solubility of quinone compounds in an aqueous electrolyte is limited in an aqueous zinc battery system, dissolved quinone salts compounds, even in small amounts, pass through the membrane/separator and react with the anode, causing rapid capacity drops.[5, 21] Therefore, the development of organic cathodes containing carbonyl groups for aqueous zinc batteries is currently underway.

Pillar[5]quinone (P5Q), which was realized for the first time in 2009, attracts great interest with the ability of multiple carbonyl groups in its structure to act as active centers during battery applications and low molecular weight per active center and theoretical capacity up to 446 mAh g^{-1}.[22] In the literature, P5Q has been employed as a cathode material in different battery types,[22a, 23] but not yet in aqueous zinc ion batteries. Herein, the

pillar[5]arene containing 1-4 dimethoxybenzene units was initially synthesized[24] and then P5Q was obtained by oxidation of the pillar[5]arene compound, according to previous reports[25] and applied for the first time as a cathode material for aqueous ZIBs. Having characterized P5Q using relevant spectroscopic techniques, its electrochemical performances were evaluated vs Zn/Zn^{2+} in 2.0 M $ZnSO_4$ aqueous electrolyte. Post-mortem structural analyses and density functional theory (DFT) calculations were used to further investigate the coordination mechanism of P5Q with Zn^{2+}/H^+ ions. Electrochemical quartz crystal microbalance with motional resistance monitoring (EQCM-R) was used to investigate the interfacial properties of the electrode during the electrochemical cycling.

Results and Discussion

P5Q was synthesized according to the literature (Scheme 1).[25] The ^1H NMR, mass spectroscopy and FT-IR spectrum were found to be compatible with the literature data (Figures S1-S4).[22a] The ^1H NMR spectrum of P5Q shows that $-CH_2$ protons in the benzoquinone rings resonate at 3.50 ppm, and the methylene bridges connected to the benzoquinone rings at the 2,5-position resonate at 6.56 ppm, in accordance with the literature. When the FT-IR (ATR, cm^{-1}) spectrum of the P5Q compound is examined, υ=1648 cm^{-1} C=O stretching vibrations, υ=1605 cm^{-1} C=C stretching vibrations of α, β unsaturated carbonyl, υ=1236 cm^{-1} are present. It has been observed that the peaks of $-CH_2$ stretching vibrations, aromatic and aliphatic -CH bending vibrations at υ= 3053 and 2963 cm^{-1} are compatible with the structure.

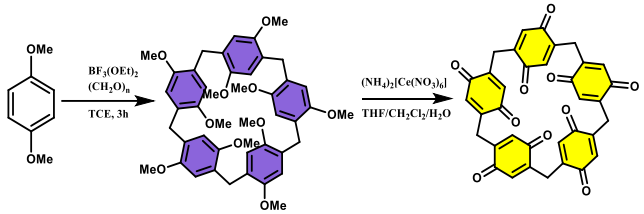

Scheme 1. Synthetic pathway of P5Q. [18, 19]

The electrochemical behaviour of P5Q/KB (30:70 w/w) electrode was investigated using cyclic voltammetry (CV) between 0.1 and 1.6 V vs. Zn/Zn^{2+} voltage range in 2.0 M $ZnSO_4$ aqueous electrolyte shown in Figure 1a. Redox peaks were observed at 1.15 and 0.95 V (vs. Zn/Zn^{2+}) for oxidation and reduction, respectively, at a scan rate of 1.0 mV s^{-1}. These overlapping peaks are attributed nominally to reversible Zn ion uptake of the quinone-based cathode P5Q. The C-rate performance of the P5Q/KB electrode has also been tested. The voltage-plateau correlated with the redox capacities were presented in Figure 1b. The P5Q cathode exhibited high discharge capacity (i.e., 100 mAh g^{-1}) at high current densities (at 500 C) with nearly 99% Coulombic efficiency (1C= 89.3 mA g^{-1}) (Figure 1c). At lower current density (i.e., 10C), lower Coulombic efficiency was obtained (~90%) associated with the irreversible proton insertion [26], it has also been demonstrated by the redox process of quinones.[17] Furthermore, following the C-rate performance shown in Figure 1c, the long-term cycling performance of the P5Q electrode at ultrafast (500 C) current density resulted in >99% Coulombic efficiency over 10000 cycles, eventually delivering a capacity value of ~120 mAh g^{-1} (Figure 1d). Then, by switching to lower current density (from 500 C to 120 C), a discharge capacity of ~182 mAh g^{-1} over 7000 cycles with a stable long-life and was achieved, exhibiting ~80% capacity retention and >99% Coulombic efficiency. In addition, high P5Q content and low carbon content (80:20 w/w) were used to compare the electrochemical performances of P5Q/KB in Figure S5. Although the P5Q/KB (80:20) electrode had the same redox behaviour as the P5Q/KB (30:70) composite electrode, the P5Q/KB (80:20) did not exhibit significant electrochemical performance above 10 C current density in the galvanostatic rate test which can be explained by the poor electrical conductivity of the quinone structures. The self-discharge behavior of the P5Q/KB electrode was also determined by monitoring the open-circuit voltage (OCV) mode after a complete cycle. For rechargeable battery systems, low self-discharge behavior is a desirable and critical characteristic. Side interactions between electrodes and electrolytes are the main reason for the self-discharge processes [27] Fig. S6 displays the time-dependent OCV profile of the Zn- ion battery based on the P5Q/KB cathode. It is apparent that following the initial voltage decline, the OCV of the P5Q/KB cathode remains constant at about 1.05 V after 13 days of relaxation time. The retention rate of the cell was calculated as 91.3% from the OCV profile at the end of 13 days. After all, it is noted that the P5Q active material has been used as cathode material in different organic electrolyte batteries,[22a, 23c] but there have been no reports on its use in aqueous electrolyte Zn ion batteries and to the best of our knowledge, among quinone-based organic cathode electrodes, the performance reported here (high current (500 C) and long cycling) stands out compared to other examples. (Table S1)[5, 28]

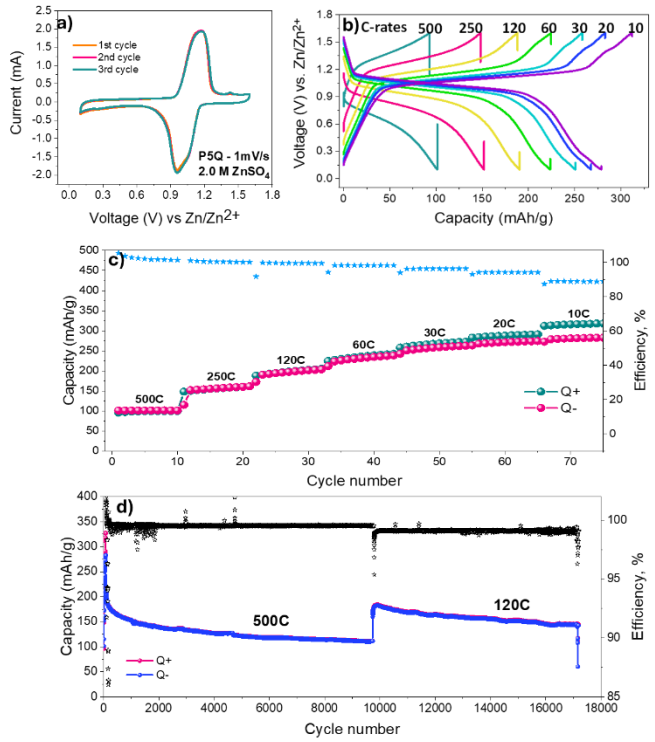

Figure 1. Electrochemical performances of P5Q electrode a) cyclic voltammetry profiles at a scan rate of 1.0 mV s^{-1}, b) galvanostatic charge/discharge performances at different current densities, c) C-rate performances from high to low current densities and d) long-term cycling performance of P5Q organic electrode after a current density of 500 C followed by a current density decrease to 120 C.

EIS analysis of P5Q/KB was also performed to obtain further electrochemical behaviour at open circuit voltage (OCV). The Nyquist diagrams in Figure S7, before and after the C-rate test for 100 cycles, represent the solution resistance as R_1, R_2 is related to the electrode/electrolyte interphase formation, R_3 is the charge transfer resistance and finally R_t is the total resistance. The EIS data for the pre-cycle were fitted and R_1 was obtained as 0.98 Ω, R_2 74.11 Ω and R_3 64.72 Ω and the total resistance R_t was calculated as 139.8 Ω. After 100 cycles, the EIS data of P5Q/KB were fitted and the values of R_1, R_2, R_3 were obtained as 1.66 Ω, 25.25 Ω and 71.4 Ω respectively (R_t: 98.31 Ω). Moreover, the Warburg impedance in the Nyquist plot gives a straight line with a 45° angle in the EIS at low frequency and can be attributed to Zn ion diffusion. The charge transfer resistance at the SEI is associated with a semicircle at high frequency. The Zn ion diffusion coefficient is estimated with Equation (1), where R is the absolute gas constant, T is the room temperature (298 K), A is the electrode surface area (1 cm^2), n is the number of electron transferred, F is the Faraday constant (96,500 C/mol), C is concentration of Zn^{2+} in the electrode material, σ is the Warburg factor which was calculated from the slope of real impedance (Z_{Re}) versus the angular frequency ($\omega^{-0.5}$) with using the Equation (2). The Zn^{2+} diffusion coefficient of P5Q/KB was determined to be $2.5 \cdot 10^{-13}$ cm^2 s^{-1} before C-rate and $8.8 \cdot 10^{-13}$ cm^2 s^{-1} after the C-rate performance, indicating that the wettability increased and the structure did not degrade after being tested.

$$D_{(Zn^{2+})} = \frac{R^2 \times T^2}{(2 \times A^2 \times n^4 \times F^4 \times C^2 \times \sigma^2)} \qquad (1)$$

$$Z_{Re} = R_s + R_{ct} + \sigma\omega^{-0.5} \qquad (2)$$

Figure S8 represents SEM images and X-ray diffraction patterns of the pristine P5Q, P5Q/KB and fully discharged P5Q/KB composite electrode. The pristine P5Q active material has fiber-shaped crystalline structure and is homogeneously covered with KB carbon resulting in amorphous network in agreement with XRD patterns. Moreover, a typical flake-like shaped of zinc sulfate hydroxide $Zn_4SO_4(OH)_6 \cdot xH_2O$ (ZHS) was also observed in SEM image of the fully discharged P5Q/KB electrode in 2.0 M $ZnSO_4$ electrolyte. The formation of ZHS in $ZnSO_4$ electrolyte is mainly caused by proton insertion into the cathode which releases OH^- ions and causes a local pH increase.[17, 29] In the XRD patterns of the fully discharged cathode, the additional new peaks that appear can be assigned to the ZHS structure as JCPDS number 00-044-0674, resulting from the participation of protons in the charge balance.[30] To further understand the formation of the ZHS structure, Energy dispersive X-ray spectroscopy (EDS) analysis was applied to the P5Q/KB and the fully discharged electrode and provided a Zn:S ratio of about 4, in agreement with the composition of $Zn_4SO_4(OH)_6 \cdot 4H_2O$ in the discharged electrode, since Zn and S were absent in the P5Q/KB active material (Figure S9).[28a, 31]

The dissolution of small molecular species in the electrolyte is the most common problem with quinones used in various battery applications, resulting capacity degradation. In aqueous battery systems, although the solubility of quinone compounds in aqueous electrolyte is low, the dissolution of discharge by-products and their reaction with the anode through the membrane/separator causes rapid capacity fading.[1, 32] The solubility of P5Q electrodes were tested in an aqueous $ZnSO_4$ solution. The pristine and discharge states of all solutions were colourless in the solution, indicating that P5Q are not dissolved in the aqueous system. UV-vis spectroscopy tests of P5Q were performed to compare their solubility and it was observed that while discharge state did not show any absorption peak, pristine state demonstrated an absorption peak at around 320 nm revealing its slight solubility in aqueous medium (Figure S10).

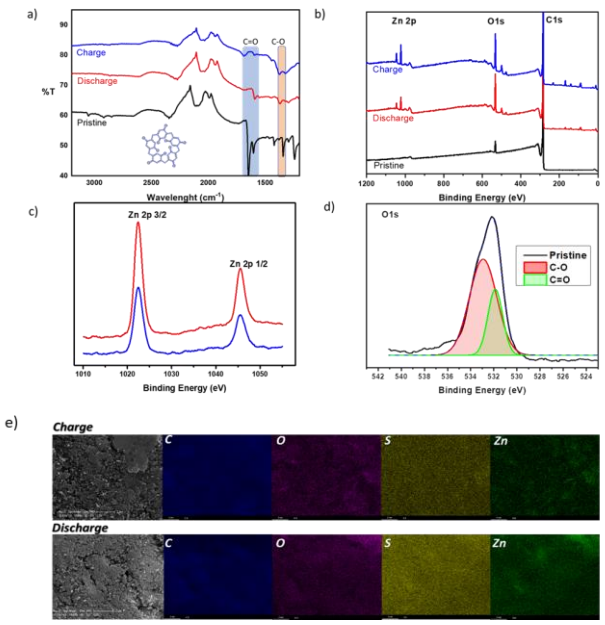

Figure 2. a) FT-IR spectra of the P5Q electrode in the pristine and first charge-discharge states, b) Ex-situ XPS spectra of the P5Q electrode in the pristine and first charge/discharge states c) Zn 2P spectra, and d) O 1S spectra e) elemental mapping images of the C, O, S and Zn components of the charge/discharge states of the P5Q: carbon (blue), oxygen (purple), sulfur (yellow), zinc (green).

FT-IR and XPS analyses investigated the structural change of carbonylated bonds in the structure of P5Q in the pristine, discharge and charged states. Ex-situ FT-IR revealed that the stretching vibration of carbonyl bonds on the benzene ring at a wavelength of C=O 1645 cm^{-1} decreased due to the enolization reaction occurring in the discharge state.[23a] Enolization formation was supported by the disappearance of the peak at 1376 cm^{-1} wavelength during charging (Figure 2a). XPS was used to further analyze the incorporation process of zinc ion into P5Q. The Zn-2p XPS spectra of the P5Q indicate the appearance of the divalent state Zn element after the first discharge (Figure 2b-c). O 1s spectrum (Figure 2d), area ratio of C=O at 531.8 eV and C-O at 532.9 eV is close to 2:1 during charging of the P5Q cathode. [33] This value is consistent with other studies reported in the literature.[23a] Zinc ion binding was also verified by scanning electron microscopy-energy dispersive X-ray spectroscopy (SEM-EDS) by mapping charged/discharged images of P5Q (Figure 2e). Both in the discharge state and in the charge state, the spatial distribution of elements C and O is similar. However, as the Zn mapping intensity changed from discharge to charge state indicating that Zn^{2+} was involved in the charge storage mechanism.

EQCM-R analysis was conducted to monitor the electrode/electrolyte interface evolution during electrochemical cycling and to further investigate the coordination mechanism of ions during the redox process. Figure 3a shows the CV and frequency variation (Δf) response of the P5Q composite thin film electrode, tested for 21 cycles at 25 mV s^{-1}. The CV profile exhibits redox peaks, aligning with the findings observed in Figure 1. The simultaneously monitored QCM resonant frequency shows a decrease/increase during the negative and the positive potential sweeps, respectively (Figure 3a), indicating a significant cation contribution to the charge storage process at a quick glance. It is well-known that these Δf patterns can be converted to mass variations (Δm) using the Sauerbrey equation[34]: $\Delta f = -k_s \times \Delta_m$, where k_s is the experimental sensitivity coefficient. However, this relationship is valid under certain conditions[35] and can be verified by monitoring the motional resistance (R_m) change during the same test. The inset in Figure 3a and S10a shows a "mirror image" relationship between the ΔR_m and Δf, as well as significantly high ΔR_m values within a cycle, which prevents us from using the QCM as a gravimetric probe. Consequently, mass per electron values (M.P.E.) calculated using Δf and ΔC from the EQCM results (not shown) lead to much higher values than that would correspond to only Zn^{2+} or proton coordination. Therefore, the Δf cannot be exclusively assigned to cation coordination/de-coordination during discharge/charge process, but intertwined with the ZHS formation/dissolution, related to the local pH changes[30, 36], as a result of coordination of H^+ with P5Q. This result is consistent with the above experimental observations (ex-situ SEM and XRD, Figure S8-9 and Figure 3) and the predictions of the DFT calculations discussed below (Figure 4). Other contributions to ΔR_m also includes the viscoelasctic property changes of the electrode during electrochemical cycling, however R_m returns to its initial value, which infer to a reversible process.

Another noteworthy observation in this analysis is related to the EQCM profiles (current and frequency) as a function of cycling. Figure 3b shows a slight upwards shift in the Δf, corresponding to a $\Delta f_{charge} - \Delta f_{discharge} > 0$ condition for the first cycles, which becomes almost zero in the following cycles, indicating a fully reversible process. The corresponding charge profile also shows a relatively low Coulombic efficiency (Figure S11b). This could mean both trapping of the charge carriers, but also exclusion of water molecules from the structure by coordination of ions to P5Q. Additionally, active material dissolution can also lead to this $\Delta f_{charge} - \Delta f_{discharge} > 0$ condition (a slight dissolution was shown in Figure S10 with UV visible experiments).

Next, we investigate the same phenomena (Δf efficiency during charge/discharge over cycling) as a function of potential scan rate. It turns out that the same observation holds, but is much more pronounced at lower scan rates, i.e., 10 mV s^{-1} (Figure 3c). Cycling these electrodes at higher rates leads to a Δf_{charge} to $\Delta f_{discharge}$ to ratio of ~1 (Figure S12). Furthermore, EQCM analyses could be performed up to 1000 mV s^{-1} (Figure 3e and 3f) which is in line with the ultra-high rate performance of the P5Q based massive electrode shown in Figure 1. Even at 1000 mV s^{-1}, we have a high ΔR_m / Δf ratio, which translates into M.P.E. values of ~425 g mol^{-1}. This observation can imply a reversible ZHS formation/dissolution, and thus a rapid proton coordination/de-

coordination. Considering that the active material dissolution is a minor effect (Figure S10, UV visible experiments), then one can still speculate that the microbalance frequency irreversibility at lower rates are related to a Zn^{2+} coordination, leading to water exclusion from the structure.

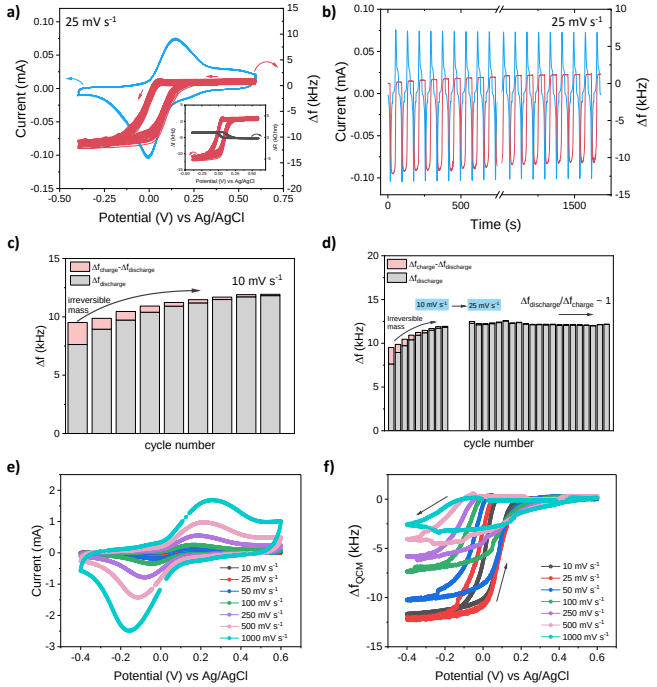

Figure 3. a) EQCM-R analyses of P5Q composite thin layer on the Au electrode of the QCM resonator, electrochemical tests are performed in 2.0 M $ZnSO_4$ electrolyte. a) CV response and frequency variation curves at 25 mV s^{-1} tested for 21 cycles, inset shows the motional resistance (R_m) change during the same test, b) shows the frequency and current response as a function of time. The panel c) shows the $\Delta f_{discharge}$ and Δf_{charge} portions of the QCM response at 10 mV s^{-1} and the panel b) shows the same analysis for consecutive cycles while changing the potential scan rate to 25 mV s^{-1}. The electrode is cycled at different scan rates (10 - 1000 mV s^{-1}), e) CV and f) the frequency response, shown for the 8th cycle.

The possible electrochemical mechanism of P5Q with Zn^{2+} and H^+ ions, was investigated by DFT calculations. The P5Q structure was optimized at B3LYP/6-31G(d,p) method and water as a solvent (IEFPCM). Firstly, the molecular electrostatic potential (MESP) for P5Q demonstrates symmetrically negative charge distributions at the top-bottom sides and positive charge distribution within the molecular gap (Figure 4a). This mapping suggests that P5Q has the ability to bond with various cations at two sites. The P5Q molecule has total of ten carbonyl groups on the opposite sides. As seen in the MESP map, there are ten binding sites for Zn^{2+}/H^+ ions in the P5Q molecule, which have theoretically identical carbonyl groups. In the optimized P5Q structure, the distance between adjacent oxygen atoms was determined to be approximately 5.1045 Å. In the optimized P5Q structure, the distance between the first Zn atom and the nearest oxygen atom (carbonyl groups in P5Q) was determined to be approximately 1.85 Å. Similarly, in the second zinc coordination, the Zn-O distance about 1.90 Å and the distance between Zn atoms is 2.03 Å (Figure 4b). Therefore, with respect to the Zn-O bond lengths and single-point energy calculation (Figure S13), it was assumed that O-Zn···Zn-O bonds may also exist. Consequently, all calculations were designated based on these interactions.

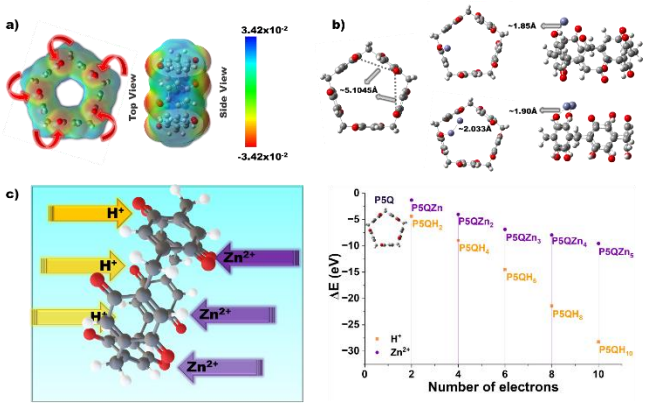

Figure 4. a) MESP of P5Q, b) The arrangement of P5Q for Zinc species and c) ΔE energy for $GP5QZn_x$ and $GP5QH_y$ species.

According to the proposed electrochemical mechanism of P5Q cathode in AZIBs, one P5Q molecule can combine with different number of Zn or H atoms. The ΔE value can be calculated by the Gibbs free energy difference between $P5QZn_{(x)}/H_{(y)}$, and the sum of Zn/H atom and $P5QZn_x$/$P5QH_y$. As seen in Figure 4c when the binding energies were calculated for pure Zn^{2+} and H^+ coordination, all ΔE values were smaller than zero, indicating that each step in which P5Q associates with a Zn or H atom can occur spontaneously. Furthermore, calculations show that pure H^+ coordination is more likely than pure Zn^{2+} coordination in the P5Q structure (Figure 4c-Table S2. Besides the current mechanism of pure Zn^{2+} or H^+ coordination, a H^+/Zn^{2+} coordination mechanism in quinone molecules is also possible.[37] Comparing the single-point energies of conformations that provide only zinc and proton coordination (n = 2, 4, 6, 8, and 10 electrons) and the single-point energies of P5QZnH species with an equal number of electrons, it appears that the formation of these structures is possible (Table S3). Protons are ions with high ionic mobility, small size and fast kinetics. Theoretical calculations have shown that relative to zinc ion coordination, proton ions can easily coordinate with the P5Q structure. Both ions tend to spontaneously bond with the P5Q structure. Considering the experimental conditions and theoretical calculations, it is thought that both ion species can coordinate competitively with the P5Q structure.

Conclusion

In this work, the P5Q structure used as a cathode in aqueous zinc ion batteries (AZIBs) has been successfully synthesized and characterized. The charge storage mechanism of the P5Q cathode and its electrochemical performance in AZIBs were extensively investigated by ex-situ characterization techniques as well as EQCM study and DFT calculations, and it has been verified that the redox reactions at the P5Q cathode are mediated by H^+/Zn^{2+} coordination. As a family of organic electrodes, P5Q is distinguished by its very fast charge-discharge characteristics. At ultrafast current densities very promising results were obtained (i.e. 120 mAh g^{-1} capacity at the end of 10000 cycles at 500 C and 182 mAh g^{-1} capacity at the end of 7000 cycles at 120C) with over 99% Coulombic efficiency. PnQ moieties are structurally similar to pillarenes and, like them, possess host-guest relationships, planar chirality and impressive electronic properties. PnQ has non-covalent interactions, thus, as the number of quinone monomers increases, the number of ion-π interactions increases. Compared to previous examples, the findings are remarkable due to the long cycling and high current density among quinone-based organic cathode electrodes. Our results indicate that pillar[n]quinones are promising cathode materials in AZIBs.

Experimental Section

Materials and methods

1,4 Dimethoxy benzene, paraformaldehyde, Ammonium Cerium (IV) Nitrate, dichloromethane, and tetrahydrofuran (THF) were purchased from Sigma-Aldrich. 1,2 dichloroethane was obtained from Fluka and Boron Trifluoride Etherate from Alfa Aesar. The deuterated solvent ($CDCl_3$-d) for NMR spectroscopy was obtained from Merck. Analytical thin layer chromatography (TLC) was performed on Silica gel plates (Merck, Kieselgel 60, 0.25 mm thickness) with F254 indicator. All reagents were purchased and directly used without being further purified.

P5Q was characterized by NMR in $CDCl_3$-D on a Varian INOVA 500-MHz spectrometer using ^{1}H NMR (Nuclear Magnetic Resonance) spectroscopy. FT-IR (Fourier-transform infrared spectroscopy) recorded on a Bruker Alpha-P in ATR in the range of 650-4000 cm^{-1}. The P5Q structural changes at the different states were investigated with X-ray photoelectron spectroscopy (XPS) analyses and recorded using a Specs Flex-Mod system with a monochromatic Al Kα X-ray source. All theoretical calculation of the P5Q structures were performed by the B3LYP functional (Becke's Three Parameter Hybrid Functional using the LYP Correlation Functional) with the 6-31G (d,p) basis set. The morphological and elemental analysis of the pristine and fully discharged P5Q/Ketjen Black (KB) were investigated by SEM (FEI PHILIPS, XL30 SFEG SEM) equipped with energy dispersive X-ray spectroscopy (EDS). X-ray diffraction of P5Q/KB and $Zn_4SO_4(OH)_6{\cdot}xH_2O$ (ZHS) structure were recorded using a Bruker-D8 Advance diffractometer (Bruker AXS).

Electrochemical Measurements

The P5Q/KB electrode was prepared by hand grinding 30 wt.% P5Q active powder and 70 wt.% KB conductive carbon in a mortar for half an hour. Galvanostatic charge-discharge (GCD) and cyclic voltammetry (CV) measurements were carried out in 2-electrode Swagelok cell at operating voltage range between (0.1 – 1.6) V vs Zn/Zn^{2+} in 2.0 M $ZnSO_4$ aqueous electrolyte via Bio-Logic VMP-3 electrochemical workstation. P5Q/KB electrode was utilized as a working electrode and zinc foil was used as both counter and reference electrode. The loading of active material was kept around 0.75- 1.0 mg per cm^2 for each electrochemical measurement. Electrochemical impedance spectroscopy (EIS) was carried out at open circuit potential (OCV) in the frequency range from 200 kHz to 1100 mHz in a 2-electrode Swagelok cell. All the electrochemical experiments were conducted at room temperature.

EQCM-R experiments were conducted employing AT-cut gold-patterned 9 MHz quartz resonators (AWS, Valencia, Spain) as piezoelectric sensors and the gold electrode acting also as the current collector. A homogeneous mixture containing the P5Q powder was prepared and coated on the gold electrode (0.2 cm^2) of the quartz resonator by drop-casting. For the slurry preparation, the P5Q has been thoroughly mixed with Ketjen Black (KB) and PVdF(Polyvinylidene fluoride) in a weight ratio of 24:56:20 (P5Q:KB:PVdF) before dispersion in NMP to ensure the binding and the electrical conductivity of the resulting composite electrode. After drop-casting, the QCM resonators were dried in a hot-plate at 80 °C. The total mass loading of the electrodes was estimated by measuring the resonant frequency of the quartz crystals before and after coating and was typically kept around 15µg for 0.2 cm^2 to be able to detect the redox signature of P5Q. The prepared electrodes were then electrochemically tested using a Bio-Logic electrochemical workstation (Bio-Logic SP200) coupled with a SEIKO QCM922A device that allows simultaneous monitoring of frequency (Δf) and the motional resistance changes (ΔR_m). The coated quartz crystals, platinum mesh and Ag/AgCl electrode were used as the working, counter, and reference electrodes, respectively. All the EQCM tests have been performed in 2.0 M $ZnSO_4$ aqueous electrolyte.

DFT calculation

Gaussian 16W software package was used for DFT (density functional theory) calculations to find the structural details of P5Q[38] To verify the optimized structures, all frequency, and single-point energy calculations were carried out at B3LYP/6-31G(d,p). Furthermore, the solvation effect was studied utilizing the integral equation formalism variation of the Polarizable Continuum Model (IEFPCM) applying water as the solvent.[39] The $\Delta E(\Delta G)$ energy was calculated by subtracting the Gibbs free energy difference between the complex's total energy

($GP5Q(M)_n$) and the sum of the individual energy of the ions (GM) and ($GP5QM_{(n-1)}$)).[40] The molecular electrostatic potential (MESP) approach was used to predict the electrostatic potential map of P5Q based on the optimal structure of the molecule (B3LYP/6-31G(d,p). Using the Gaussian View 6, the MESP analysis was also performed to determine possible active sides for Zn^{2+}/H^+ coordination.

Supporting Information

Supporting information is available online.

Acknowledgements

The authors acknowledge the financial support of the TÜBİTAK 222Z042 project and thank the TÜBİTAK ULAKBIM, High Performance and Grid Computing Center (TR-Grid e-Infrastructure) for calculations in the computational chemistry details of this paper. YS expresses her gratitude to TÜBİTAK 2211-A Domestic Doctoral Fellowship Program and Higher Education Council (YÖK) 100/2000 Doctoral Fellowship Program for their financial support. BU is indebted to TÜBİTAK 2211-C Domestic Priority Areas Doctoral Fellowship Program and Higher Education Council (YÖK) 100/2000 Doctoral Fellowship Program for their support.

Keywords: Aqueous zinc ion batteries, organic cathode, pillar[5] quinone, electrode/electrolyte interface

References

[1] G. Fang, J. Zhou, A. Pan, S. Liang, *ACS Energy Letters* **2018**, *3*, 2480-2501.

[2] S. Lee, G. Kwon, K. Ku, K. Yoon, S.-K. Jung, H.-D. Lim, K. Kang, *Advanced Materials* **2018**, *30*, 1704682.

[3] P. Yu, Y. Zeng, H. Zhang, M. Yu, Y. Tong, X. Lu, *Small* **2019**, *15*, 1804760.

[4] H. Cui, L. Ma, Z. Huang, Z. Chen, C. Zhi, *SmartMat* **2022**, *3*, 565-581.

[5] Q. Zhao, W. Huang, Z. Luo, L. Liu, Y. Lu, Y. Li, L. Li, J. Hu, H. Ma, J. Chen, *Science Advances*, *4*, eaao1761.

[6] C. Han, H. Li, R. Shi, T. Zhang, J. Tong, J. Li, B. Li, *Journal of Materials Chemistry A* **2019**, *7*, 23378-23415.

[7] Y. Lu, J. Chen, *Nature Reviews Chemistry* **2020**, *4*, 127-142.

[8] S. Yeşilot, S. Küçükköylü, T. Mutlu, R. Demir-Cakan, *Energy Technology* **2021**, *9*, 2100563.

[9] Z. Tie, Z. Niu, *Angewandte Chemie (International ed. in English)* **2020**, *59*, 21293-21303.

[10] M. Na, Y. Oh, H. R. Byon, *Chemistry of Materials* **2020**, *32*, 6990-6997.

[11] Z. Tie, L. Liu, S. Deng, D. Zhao, Z. Niu, *Angewandte Chemie (International ed. in English)* **2020**, *59*, 4920-4924.

[12] S. Wang, S. Huang, M. Yao, Y. Zhang, Z. Niu, *Angewandte Chemie (International ed. in English)* **2020**, *59*, 11800-11807.

[13] a) H. Yi, Y. Ma, S. Zhang, B. Na, R. Zeng, Y. Zhang, C. Lin, *ACS Sustainable Chemistry & Engineering* **2019**, *7*, 18894-18900; b) H. Yu, G. Liu, M. Wang, R. Ren, G. Shim, J. Y. Kim, M. X. Tran, D. Byun, J. K. Lee, *ACS Applied Materials & Interfaces* **2020**, *12*, 5820-5830; c) Y. Ma, X. Xie, R. Lv, B. Na, J. Ouyang, H. Liu, *ACS Sustainable Chemistry & Engineering* **2018**, *6*, 8697-8703.

[14] a) T. Sun, J. Xie, W. Guo, D.-S. Li, Q. Zhang, **2020**, *10*, 1904199; b) K. Zhang, K. O. Kirlikovali, R. S. Varma, Z. Jin, H. W. Jang, O. K. Farha, M. Shokouhimehr, *ACS Appl Mater Interfaces* **2020**, *12*, 27821-27852.

[15] a) X. Feng, X. Ding, D. Jiang, *Chemical Society Reviews* **2012**, *41*, 6010-6022; b) A. P. Côté, A. I. Benin, N. W. Ockwig, M. O'Keeffe, A. J. Matzger, O. M. Yaghi, *Science (New York, N.Y.)* **2005**, *310*, 1166-1170.

[16] W. Wang, V. S. Kale, Z. Cao, Y. Lei, S. Kandambeth, G. Zou, Y. Zhu, E. Abouhamad, O. Shekhah, L. Cavallo, M. Eddaoudi, H. N. Alshareef, *Advanced Materials* **2021**, *33*, 2103617.

[17] Z. Lin, H.-Y. Shi, L. Lin, X. Yang, W. Wu, X. Sun, *Nature Communications* **2021**, *12*, 4424.

[18] J. Cui, Z. Guo, J. Yi, X. Liu, K. Wu, P. Liang, Q. Li, Y. Liu, Y. Wang, Y. Xia, J. Zhang, *ChemSusChem* **2020**, *13*, 2160-2185.

[19] D. Kundu, P. Oberholzer, C. Glaros, A. Bouzid, E. Tervoort, A. Pasquarello, M. Niederberger, *Chemistry of Materials* **2018**, *30*, 3874-3881.

[20] Z. Guo, Y. Ma, X. Dong, J. Huang, Y. Wang, Y. Xia, *Angewandte Chemie International Edition* **2018**, *57*, 11737-11741.

[21] S. Huang, J. Zhu, J. Tian, Z. Niu, *Chemistry (Weinheim an der Bergstrasse, Germany)* **2019**, *25*, 14480-14494.

[22] a) W. Xiong, W. Huang, M. Zhang, P. Hu, H. Cui, Q. Zhang, *Chemistry of Materials* **2019**, *31*, 8069-8075; b) D. Cao, Y. Kou, J. Liang, Z. Chen, L. Wang, H. Meier, *Angewandte Chemie International Edition* **2009**, *48*, 9721-9723.

[23] a) W. Zhang, H. Tian, J. Wang, H. Sun, J. Wang, W. Huang, *ACS Applied Materials & Interfaces* **2022**, *14*, 38887-38894; b) H. Sun, W. Xiong, W. Zhou, W. Zhang, L. Wang, W. Huang, *Organic Electronics* **2020**, *83*, 105743; c) Z. Zhu, M. Hong, D. Guo, J. Shi, Z. Tao, J. Chen, *Journal of the American Chemical Society* **2014**, *136*, 16461-16464.

[24] T. Ogoshi, S. Kanai, S. Fujinami, T.-a. Yamagishi, Y. Nakamoto, *Journal of the American Chemical Society* **2008**, *130*, 5022-5023.

[25] D. N. Shurpik, P. L. Padnya, L. I. Makhmutova, L. S. Yakimova, I. I. Stoikov, *New Journal of Chemistry* **2015**, *39*, 9215-9220.

[26] a) N. Makivić, K. D. Harris, J.-M. Tarascon, B. Limoges, V. Balland, *Advanced Energy Materials* **2023**, *13*, 2203122; b) N. Makivić, J.-Y. Cho, K. D. Harris, J.-M. Tarascon, B. Limoges, V. Balland, *Chemistry of Materials* **2021**, *33*, 3436-3448; c) R. Emanuelsson, M. Sterby, M. Strømme, M. Sjödin, *Journal of the American Chemical Society* **2017**, *139*, 4828-4834.

[27] a) T. Mutlu, R. Demir-Cakan, *Electrochimica Acta* **2021**, *390*, 138825; b) Z. Huang, T. Wang, H. Song, X. Li, G. Liang, D. Wang, Q. Yang, Z. Chen, L. Ma, Z. Liu, B. Gao, J. Fan, C. Zhi, *Angewandte Chemie (International ed. in English)* **2021**, *60*, 1011-1021.

[28] a) N. Kılıç, S. Yeşilot, S. Sariyer, A. Ghosh, A. Kılıç, O. Sel, R. Demir-Cakan, *Materials Today Energy* **2023**, *33*, 101280; b) Y. Wang, C. Wang, Z. Ni, Y. Gu, B. Wang, Z. Guo, Z. Wang, D. Bin, J. Ma, Y. Wang, *Advanced Materials* **2020**, *32*, 2000338; c) Y. Chen, J. Li, Q. Zhu, K. Fan, Y. Cao, G. Zhang, C. Zhang, Y. Gao, J. Zou, T. Zhai, C. Wang, *Angewandte Chemie (International ed. in English)* **2022**, *61*, e202116289.

[29] B. Lee, H. R. Seo, H. R. Lee, C. S. Yoon, J. H. Kim, K. Y. Chung, B. W. Cho, S. H. Oh, *ChemSusChem* **2016**, *9*, 2948-2956.

[30] S. Sariyer, A. Ghosh, S. N. Dambasan, E. M. Halim, M. El Rhazi, H. Perrot, O. Sel, R. Demir-Cakan, *ACS Applied Materials & Interfaces* **2022**, *14*, 8508-8520.

[31] S. Sariyer, S. Yeşilot, N. Kılıç, A. Ghosh, O. Sel, R. Demir-Cakan, *Batteries & Supercaps* **2023**, *6*, e202200529.

[32] J. Xie, H. Shi, C. Shen, L. Huan, M. He, M. Chen, *Journal of Chemical Sciences* **2021**, *133*, 2.

[33] a) G.-F. Han, F. Li, W. Zou, M. Karamad, J.-P. Jeon, S.-W. Kim, S.-J. Kim, Y. Bu, Z. Fu, Y. Lu, S. Siahrostami, J.-B.

Baek, *Nature Communications* **2020**, *11*, 2209; b) Z. Tian, V. S. Kale, Y. Wang, S. Kandambeth, J. Czaban-Jóźwiak, O. Shekhah, M. Eddaoudi, H. N. Alshareef, *J Am Chem Soc* **2021**, *143*, 19178-19186; c) X. Xu, S. Zhang, K. Xu, H. Chen, X. Fan, N. Huang, *J Am Chem Soc* **2023**, *145*, 1022-1030; d) Y. Lin, K.-H. Wu, Q. Lu, Q. Gu, L. Zhang, B. Zhang, D. Su, M. Plodinec, R. Schlögl, S. Heumann, *Journal of the American Chemical Society* **2018**, *140*, 14717-14724; e) Y. Zhao, Y. Huang, H. Zhu, Q. Zhu, Y. Xia, *J Am Chem Soc* **2016**, *138*, 16645-16654; f) J. Li, S. Song, J. Meng, L. Tan, X. Liu, Y. Zheng, Z. Li, K. W. K. Yeung, Z. Cui, Y. Liang, S. Zhu, X. Zhang, S. Wu, *Journal of the American Chemical Society* **2021**, *143*, 15427-15439; g) K. W. Nam, H. Kim, Y. Beldjoudi, T.-w. Kwon, D. J. Kim, J. F. Stoddart, *Journal of the American Chemical Society* **2020**, *142*, 2541-2548; h) X. Hu, L. Zhong, C. Shu, Z. Fang, M. Yang, J. Li, D. Yu, *Journal of the American Chemical Society* **2020**, *142*, 4621-4630.

[34] G. Sauerbrey, *Zeitschrift für Physik* **1959**, *155*, 206-222.

[35] A. R. Hillman, *Journal of Solid State Electrochemistry* **2011**, *15*, 1647-1660.

[36] A. O. Efremova, A. I. Volkov, E. G. Tolstopyatova, V. V. Kondratiev, *Journal of Alloys and Compounds* **2022**, *892*, 162142.

[37] X. Deng, J. K. Sarpong, G. Zhang, J. Hao, X. Zhao, L. Li, H. Li, C. Han, B. Li, *InfoMat* **2023**, *5*, e12382.

[38] M. J. Frisch, G. W. Trucks, H. B. Schlegel, G. E. Scuseria, M. A. Robb, J. R. Cheeseman, G. Scalmani, V. Barone, G. A. Petersson, H. Nakatsuji, X. Li, M. Caricato, A. V. Marenich, J. Bloino, B. G. Janesko, R. Gomperts, B. Mennucci, H. P. Hratchian, J. V. Ortiz, A. F. Izmaylov, J. L. Sonnenberg, Williams, F. Ding, F. Lipparini, F. Egidi, J. Goings, B. Peng, A. Petrone, T. Henderson, D. Ranasinghe, V. G. Zakrzewski, J. Gao, N. Rega, G. Zheng, W. Liang, M. Hada, M. Ehara, K. Toyota, R. Fukuda, J. Hasegawa, M. Ishida, T. Nakajima, Y. Honda, O. Kitao, H. Nakai, T. Vreven, K. Throssell, J. A. Montgomery Jr., J. E. Peralta, F. Ogliaro, M. J. Bearpark, J. J. Heyd, E. N. Brothers, K. N. Kudin, V. N. Staroverov, T. A. Keith, R. Kobayashi, J. Normand, K. Raghavachari, A. P. Rendell, J. C. Burant, S. S. Iyengar, J. Tomasi, M. Cossi, J. M. Millam, M. Klene, C. Adamo, R. Cammi, J. W. Ochterski, R. L. Martin, K. Morokuma, O. Farkas, J. B. Foresman, D. J. Fox, Wallingford, CT, **2016**.

[39] X. Wang, L. Chen, F. Lu, J. Liu, X. Chen, G. Shao, *ChemElectroChem* **2019**, *6*, 3644-3647.

[40] a) M. Zhang, Y. Zhang, W. Huang, Q. Zhang, *Batteries & Supercaps* **2020**, *3*, 476-487; b) W. Yang, H. Yang, H. Zhou, *Batteries & Supercaps* **2022**, *5*, e202200197.